

Signatures of dyons and calorons in lattice gluodynamics and QCD at nonzero temperature

E.-M. Ilgenfritz¹

¹Joint Institute for Nuclear Research, BLTP, Dubna, Russian Federation

Delta-16 Workshop

Institute of Theoretical Physics, Heidelberg University
Heidelberg, April 28 – 30, 2016

most work done in collaboration with M. Müller-Preussker[†] (HU Berlin),
B. V. Martemyanov (ITEP and MEPHl Moscow) and V. G. Bornyakov
(IHEP Protvino, ITEP Moscow and Far East Federal Univ. Vladivostok)

Outline

- 1 Introduction: Cooling and vacuum structure
- 2 Conditions for “freeze-out” of numerical solutions for SU(2)
- 3 Analytical caloron and dyon solutions (for arbitrary SU(N))
- 4 Conditions for “freeze-out” of SU(3) calorons and dyons
- 5 Why calorons ? Can calorons generate confinement ?
- 6 Overlap analysis of dyon structure in gluodynamics below/above T_{dec}
- 7 Overlap analysis of dyon structure in dynamical QCD at/above T_{χ}
- 8 Outlook and Plans

Outline

- 1 Introduction: Cooling and vacuum structure
- 2 Conditions for “freeze-out” of numerical solutions for SU(2)
- 3 Analytical caloron and dyon solutions (for arbitrary SU(N))
- 4 Conditions for “freeze-out” of SU(3) calorons and dyons
- 5 Why calorons ? Can calorons generate confinement ?
- 6 Overlap analysis of dyon structure in gluodynamics below/above T_{dec}
- 7 Overlap analysis of dyon structure in dynamical QCD at/above T_x
- 8 Outlook and Plans

Outline

- 1 Introduction: Cooling and vacuum structure
- 2 Conditions for “freeze-out” of numerical solutions for SU(2)
- 3 Analytical caloron and dyon solutions (for arbitrary SU(N))
- 4 Conditions for “freeze-out” of SU(3) calorons and dyons
- 5 Why calorons ? Can calorons generate confinement ?
- 6 Overlap analysis of dyon structure in gluodynamics below/above T_{dec}
- 7 Overlap analysis of dyon structure in dynamical QCD at/above T_{χ}
- 8 Outlook and Plans

Outline

- 1 Introduction: Cooling and vacuum structure
- 2 Conditions for “freeze-out” of numerical solutions for SU(2)
- 3 Analytical caloron and dyon solutions (for arbitrary SU(N))
- 4 Conditions for “freeze-out” of SU(3) calorons and dyons
- 5 Why calorons ? Can calorons generate confinement ?
- 6 Overlap analysis of dyon structure in gluodynamics below/above T_{dec}
- 7 Overlap analysis of dyon structure in dynamical QCD at/above T_x
- 8 Outlook and Plans

Outline

- 1 Introduction: Cooling and vacuum structure
- 2 Conditions for “freeze-out” of numerical solutions for SU(2)
- 3 Analytical caloron and dyon solutions (for arbitrary SU(N))
- 4 Conditions for “freeze-out” of SU(3) calorons and dyons
- 5 Why calorons ? Can calorons generate confinement ?
- 6 Overlap analysis of dyon structure in gluodynamics below/above T_{dec}
- 7 Overlap analysis of dyon structure in dynamical QCD at/above T_{χ}
- 8 Outlook and Plans

Outline

- 1 Introduction: Cooling and vacuum structure
- 2 Conditions for “freeze-out” of numerical solutions for SU(2)
- 3 Analytical caloron and dyon solutions (for arbitrary SU(N))
- 4 Conditions for “freeze-out” of SU(3) calorons and dyons
- 5 Why calorons ? Can calorons generate confinement ?
- 6 Overlap analysis of dyon structure in gluodynamics below/above T_{dec}
- 7 Overlap analysis of dyon structure in dynamical QCD at/above T_{χ}
- 8 Outlook and Plans

Outline

- 1 Introduction: Cooling and vacuum structure
- 2 Conditions for “freeze-out” of numerical solutions for SU(2)
- 3 Analytical caloron and dyon solutions (for arbitrary SU(N))
- 4 Conditions for “freeze-out” of SU(3) calorons and dyons
- 5 Why calorons ? Can calorons generate confinement ?
- 6 Overlap analysis of dyon structure in gluodynamics below/above T_{dec}
- 7 Overlap analysis of dyon structure in dynamical QCD at/above T_{χ}
- 8 Outlook and Plans

Outline

- 1 Introduction: Cooling and vacuum structure
- 2 Conditions for “freeze-out” of numerical solutions for SU(2)
- 3 Analytical caloron and dyon solutions (for arbitrary SU(N))
- 4 Conditions for “freeze-out” of SU(3) calorons and dyons
- 5 Why calorons ? Can calorons generate confinement ?
- 6 Overlap analysis of dyon structure in gluodynamics below/above T_{dec}
- 7 Overlap analysis of dyon structure in dynamical QCD at/above T_{χ}
- 8 Outlook and Plans

Outline

- 1 Introduction: Cooling and vacuum structure
- 2 Conditions for “freeze-out” of numerical solutions for SU(2)
- 3 Analytical caloron and dyon solutions (for arbitrary SU(N))
- 4 Conditions for “freeze-out” of SU(3) calorons and dyons
- 5 Why calorons ? Can calorons generate confinement ?
- 6 Overlap analysis of dyon structure in gluodynamics below/above T_{dec}
- 7 Overlap analysis of dyon structure in dynamical QCD at/above T_{χ}
- 8 Outlook and Plans


Our first traces in Lattice Gauge Theory

Searching instanton effects (in heavy quark potential, Polyakov loop distributions, testifying the onset of deconfinement interpreted by instanton suppression) have been the main motivation to start lattice simulations in Dubna in 1980/1981.

Two well-cited papers accompanying the start of our lattice activity :

- Statistical Mechanics of the Interacting Yang-Mills Instanton Gas, E.-M. I., M. Müller-Preussker (Dubna, JINR), Nucl. Phys. B184 (1981) 443
- SU(3) Gluon Condensate From Lattice (Monte Carlo) Data, E.-M. I., M. Müller-Preussker (Dubna, JINR), Phys. Lett. B119 (1982) 395

1985: a first paper together with “western” co-authors :

- First Evidence for the Existence of Instantons in the Quantized SU(2) Lattice Vacuum, E.-M. I. (Leipzig U.), M. L. Laursen (DESY), G. Schierholz (DESY), M. Müller-Preussker (Humboldt U. Berlin), H. Schiller (IfH Zeuthen), Nucl. Phys. B268 (1986) 693 

Are these really Instantons ?

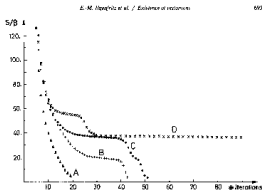


Fig. 1. The ratio S/B as a function of the number of iterations for 4 typical gauge field configurations at $\beta = 2.1$. The first iteration with $S/B > 100$ is not shown.

where r is a normalization constant such that

$$\tilde{E}_{\text{vac}} = \text{SU}(2). \quad (3)$$

When all link matrices have been changed once, we call this one iteration. This procedure will locally minimize the action. One can also think of other methods of “cooling” the gauge field configurations. A similar algorithm can also be given for $\text{SU}(3)$ [10].

Our sample of vacuum configurations consist of 40 configurations at $\beta = 2.1$ and 18 configurations at $\beta = 2.2$ on a 6^4 lattice. In Fig. 1 we have shown the history of 4 typical gauge field configurations under successive relaxations. While configurations A decays into the trivial ($S = 0$) vacuum, configurations B, C, and D show a plateau, indicating the passage through a quasi-stable field configuration. On the plateau the action takes the value

$$S = \beta(2e^2 - \Delta)N, \quad N = 1, 2, \dots, \quad (4)$$

with $\Delta = 1$. This is in close agreement with what one would expect for a continuum (anti-)instanton field configuration, i.e. $S = \beta 2\pi^2 N$. The fact that the lattice action

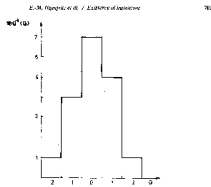


Fig. 4. Distribution of the background topological charge for the lattice of configurations at $\beta = 2.2$.

14. FERMION ZERO MODES

The lattice action for massless Kogut-Susskind fermions in a background field configuration $\{U_{\mu,\nu}\}$ is given by

$$S_f = \bar{\chi} M(\chi) = \sum_{\mu,\nu} \left[\bar{\chi}_{\nu} (-1)^{\nu_1 + \dots + \nu_{d-1}} \gamma_{\nu} \chi_{\nu} - \bar{\chi}_{\nu} \chi_{\nu} \right]. \quad (12)$$

where $\bar{\chi}_{\nu}, \chi_{\nu}$ are single component, colour doublet Grassmann variables sitting at the sites $\nu = (\nu_1, \nu_2, \dots, \nu_d)$. We assume antiperiodic boundary conditions in all 4 directions. S_f then has an explicit chiral symmetry for which $\langle \bar{\chi} \chi \rangle$ is an order parameter. In the infinite lattice volume limit we have [11]

$$\langle \bar{\chi} \chi \rangle = 2e \langle \rho(\lambda) \rangle, \quad (13)$$

where $\rho(\lambda)$ is the density of eigenvalues $\{\lambda\}$ of the fermion matrix $M(\chi)$. It is thus the existence of zero modes that will determine whether chiral symmetry is broken spontaneously or not.

In the continuum the Atiyah-Singer index theorem [16] states that the number of zero modes, Z , of self-dual or anti-self-dual gauge fields is equal to $|Q|$. To check this we have computed the eigenvalues of the fermion matrix associated with the quasi-stable field configurations using the Lanczos algorithm developed in ref. [15].

Are these really Instantons ?

702

E. M. Ilgenfritz et al. / Evidence of instantons

On a finite lattice we will, of course, not find exact zero modes, but (at most) small eigenvalues which are well separated from the rest of them. On the plaquette we found

$$Z = |Q - N| \quad (14)$$

in accordance with the index theorem. To illustrate this, we have plotted $\rho(\lambda)$ for 3 typical field configurations in fig. 5a-c. Configuration E, which has

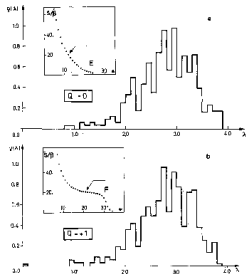


Fig. 5. (a-c) The eigenvalue density $\rho(\lambda)$ as a function of λ , for 3 typical gauge field configurations on $\beta = 2.2$. The insets show the corresponding Z/N as a function of the number of iterations, and the arrow indicates which $\lambda(\lambda)$ and Q were computed. (d) The eigenvalue density $\rho(\lambda)$ for a typical high- β configuration.

E. M. Ilgenfritz et al. / Evidence of instantons

703

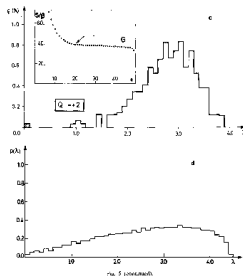


Fig. 5 (continued)

$Q = 0$, has also no "zero" mode. Configuration F, which has $Q = -1$, has one "zero" mode (not counting the degeneracy of the eigenvalues due to the fermion doubling), while configuration G, which has $Q = 1$, supports exactly 2 "zero" modes.

For comparisons we have also shown $\rho(\lambda)$ for a typical equilibrium configuration (that of fig. 5d) in fig. 5d. The difference in the two eigenvalue spectra is striking: while $\rho(\lambda)$ extends continuously to $\lambda = 0$ for the equilibrium configuration, it develops a gap in the process of relaxation leaving behind the "zero" modes.


To conclude this section, we may say that the quasi-stable field configurations underlying the equilibrium configurations have passed all tests so that they can be interpreted as (multi-) instantons. It would be interesting now to compare these

What cooling can and what it cannot

Already here the essentials have been demonstrated :

- cooling curves, plateaus of action and topological charge
- lumpy structure, description of the shape of lumps
- distribution of the number of separate lumps
- topological charge distribution (topologically, in one configuration, all lumps are of the same sign: only for cooling plateaus)
- Atiyah-Singer index theorem (in the simpler form $Q_{\text{top}} = \pm N_{\text{zm}}$)
- fermion spectrum contrasted with the spectrum in the vacuum (at that time using staggered fermions)

Now we know, however :

- Cooling doesn't act in a locally restricted way, it creates coherence over an ever increasing region of spacetime.
- Cooling finally ends up with "typical" topological configurations.
- They are at best "typical for the vacuum", but not the vacuum itself.
- This has been clarified by filtering : with access to all modes, the chirally exact overlap Dirac operator is able to "see" all scales. 

There is a one-to-one mapping between filtering and cooling steps

This has been clarified in two later papers together with QCDSF :

- Exploring the structure of the quenched QCD vacuum with overlap fermions,
E.-M. I. (Humboldt U., Berlin), K. Koller (Munich U.), Y. Koma (Mainz U., Inst. Kernphys.), G. Schierholz (DESY and NIC, Zeuthen), T. Streuer (Kentucky U.), V. Weinberg (DESY, Zeuthen and Freie U. Berlin), Phys. Rev. D76 (2007) 034506
- Vacuum structure revealed by over-improved stout-link smearing compared with the overlap analysis for quenched QCD,
E.-M. I., D. Leinweber, P. Moran (Adelaide U.), K. Koller (Munich U.), G. Schierholz (NIC, Zeuthen and DESY), V. Weinberg (NIC, Zeuthen and Freie U. Berlin), Phys. Rev. D77 (2008) 074502, err. 099902

The message from this overlap study

- The views provided by variable filtering can be reproduced by controlled cooling (e.g. at different numbers of cooling steps).
- The topological picture changes considerably with the resolution scale (in parlance of today: Wilson flow time).
- laminar structure and topological lumps co-exist, however each structure living at its own scale (these are very different ones) !
- Instantons and/or calorons and dyons become characteristic at the infrared scale !
- Therefore potentially interesting for model building.
- Do they provide a mechanism for confinement ?

The role of holonomy

The importance and usefulness of the finite-temperature holonomy (considered globally to distinguish the phases of the theory and locally to distinguish different “dyonic” constituents (or “instanton quarks”) for studies of the topological structure was recognized for the first time through the discovery of the Kran-van-Baal-Lee-Lu caloron solutions. Fractional instantons (“instanton quarks”) have been imagined since long as a viable confinement mechanism. Topological charge is not their single characteristic property !
D. Diakonov : Confining dyon gases.

For confinement via $SU(2)$ dyons:
See recent papers by Ed Shuryak et al.

Outline

- 1 Introduction: Cooling and vacuum structure
- 2 Conditions for “freeze-out” of numerical solutions for SU(2)**
- 3 Analytical caloron and dyon solutions (for arbitrary SU(N))
- 4 Conditions for “freeze-out” of SU(3) calorons and dyons
- 5 Why calorons ? Can calorons generate confinement ?
- 6 Overlap analysis of dyon structure in gluodynamics below/above T_{dec}
- 7 Overlap analysis of dyon structure in dynamical QCD at/above T_{χ}
- 8 Outlook and Plans

Lattice set-up for our caloron and dyon “discovery” in 2001/2002 for SU(2) LGT

We have simulated SU(2) LGT at finite temperature on lattices $N_S^3 \times N_T$ with $N_S = 16$ or 24 and $N_T = 4$.

β values chosen as $\beta = 2.20, 2.25$ and 2.30 .

For $N_T = 4$ the phase transition is at $\beta_c = 2.299$.

Two temperatures below T_c , the other very close to T_c .

Standard Wilson action for generating configurations, standard Wilson cooling has been applied to a selection of MC configurations.

Our focus at lowest action plateaus at $S = (0.5 \dots 1.5) S_{\text{inst}}$

Also higher plateaus have been considered: multi-dyon states

Boundary conditions for gluon fields :

- always periodic in time
- periodic in space
- alternatively fixed holonomy boundary in space (periodic but timelike links on boundary kept “frozen”)

Set-up for Wilson cooling (2001/2002)

Monitoring by simple local 3D observables/Wilson-Dirac operator :

- Wilson action $\mathcal{S}(\vec{X}) = \frac{1}{N_\tau} \sum_t \mathbf{s}(\vec{X}, t)$
- topological density

$$q_{\text{top}}(\vec{X}) = \frac{1}{N_\tau} \frac{1}{2^4 32 \pi^2} \sum_t \left(\sum_{\mu, \nu, \rho, \sigma = \pm 1}^{\pm 4} \text{tr} [U_{X, \mu\nu} U_{X, \rho\sigma}] \right)$$
- Polyakov loop $L(\vec{X}) = \frac{1}{2} \text{tr} \prod_{t=1}^{N_\tau} U_{\vec{X}, t, 4}$
- spectrum of the non-Hermitian Wilson-Dirac operator

$$D_{Xr\alpha, Ys\beta} = \delta_{xy} \delta_{rs} \delta_{\alpha\beta} - \kappa \sum_{\mu} \left\{ \delta_{x+\hat{\mu}, y} (\mathbf{1} - \gamma^{\mu})_{rs} (U_{X, \mu})_{\alpha\beta} + \delta_{y+\hat{\mu}, x} (\mathbf{1} + \gamma^{\mu})_{rs} (U_{y, \mu}^{\dagger})_{\alpha\beta} \right\}$$

Stopping criteria for cooling :

- $S_n < 1.5 S_{\text{inst}}$
- $|S_n - S_{n-1}| < 0.01$
- $S_n - 2S_{n-1} + S_{n-2} < 0$ point of inflection of the cooling curve

Results

For each β , **approximately $\mathcal{O}(200)$ configurations** have been obtained by cooling in the lowest action bin.

In addition : **global “event shape observables”** have been introduced. For example, the **“non-staticity”**:

$$\delta_t = \frac{\sum_{t=1}^{N_\tau} \sum_{\vec{x}} \sum_{\mu < \nu} |\mathbf{s}(\vec{x}, t; \mu, \nu) - \mathbf{s}(\vec{x}, t-1; \mu, \nu)|}{\sum_{t=1}^{N_\tau} \sum_{\vec{x}} \sum_{\mu < \nu} \mathbf{s}(\vec{x}, t; \mu, \nu)}$$

with the local action per plane $\mathbf{s}(\vec{x}, t; \mu, \nu) = \beta \left(1 - \frac{1}{2} \text{tr} U_{x, \mu\nu}\right)$

Thus, a rough classification becomes possible :

- $\delta_t < 0.27$ are *DD* objects (two maxima of 3D action)
- $\delta_t > 0.27$ are *CAL* objects (one maximum of 3D action)

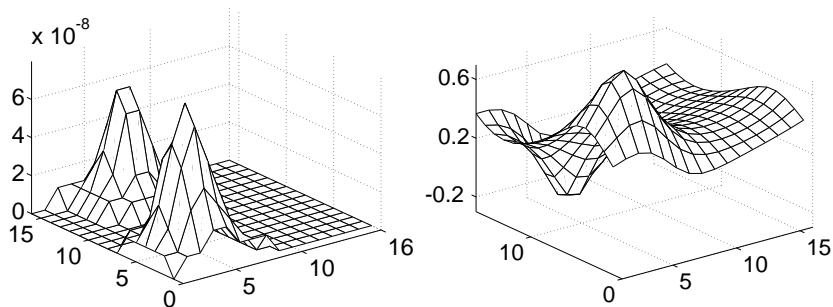
First cooling portraits of a large SU(2) caloron: *DD*

Figure: Topological charge density (left) and the Polyakov loop (right) for *DD* configurations.

Jump of the Dirac “zero mode” (single real eigenvalue)

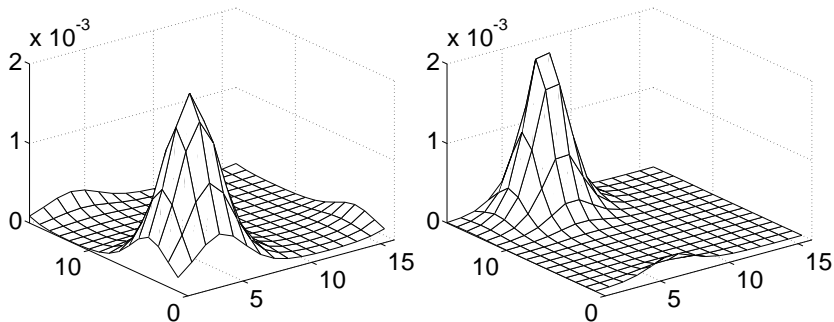


Figure: Location of the real mode corresponding to time-periodic boundary condition (left) and time-antiperiodic boundary condition (right) is moving for DD configurations

A moving real eigenvalue of the Wilson-Dirac operator with changing BC for DD

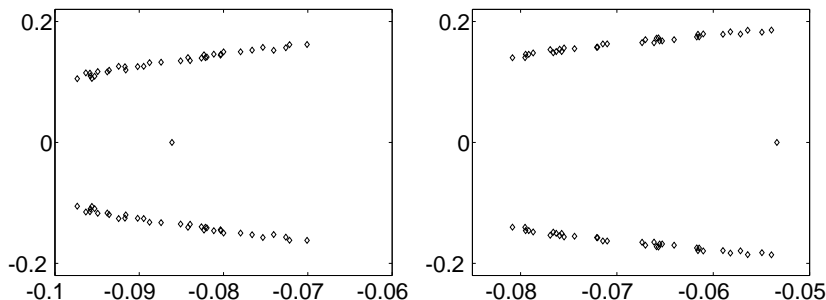


Figure: Location of the single real eigenvalue in the complex plane corresponding to time-periodic boundary condition (left) and time-antiperiodic boundary condition (right) is also moving along the real axis for DD configurations.

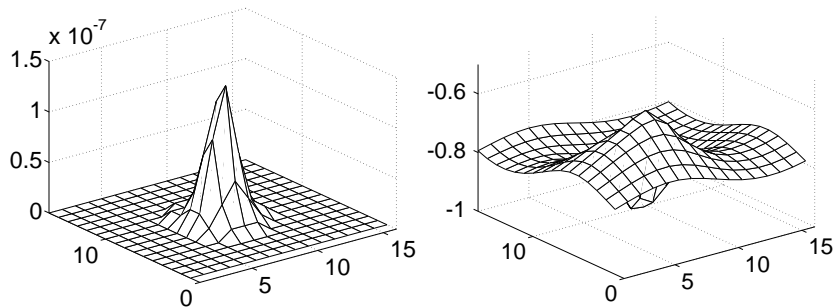
First cooling portraits of a small SU(2) caloron: *CAL*

Figure: Topological charge density (left) forming a single peak and the Polyakov loop (right) but still with "dipole" profile for *CAL* configurations.

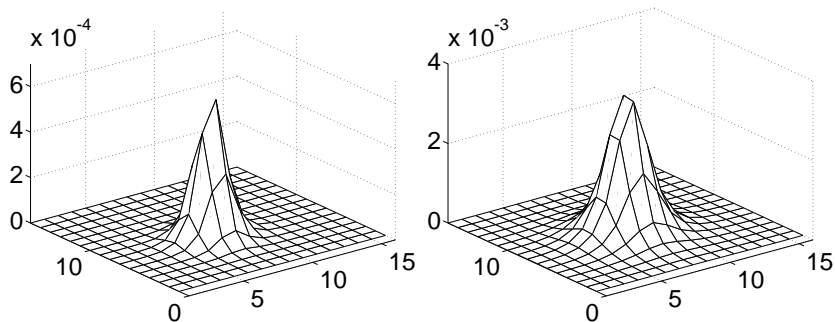
Almost no jump of the Dirac “zero mode” for *CAL*

Figure: The location of the real mode corresponding to time-periodic boundary condition (left) and time-antiperiodic boundary condition (right) is practically not changing with BC, the IPR may slightly change for *CAL* configurations.

BC-independent real eigenvalue of the Wilson-Dirac operator for *CAL* configurations.

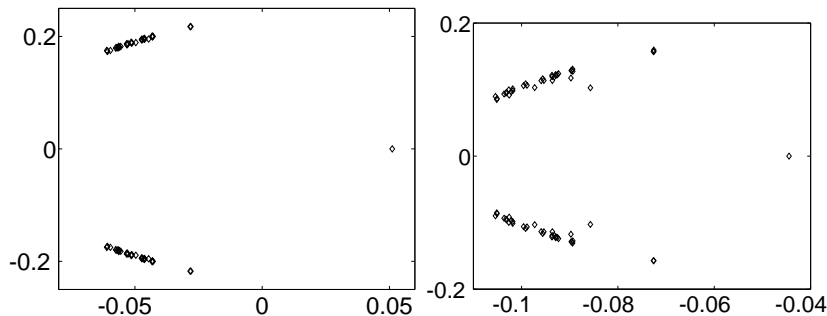


Figure: Location of the single real eigenvalue in the complex plane independent of choosing time-periodic boundary condition (left) or time-antiperiodic boundary condition (right) for *CAL* configurations.

Abundance of lowest action states found on $16^3 \times 4$

Type of solution	Boundary condition	$\beta = 2.20$	$\beta = 2.25$	$\beta = 2.30 \simeq \beta_c$
<i>DD</i>	f.h.b.c.	0.46 ± 0.05	0.52 ± 0.05	0.45 ± 0.05
	p.b.c.	0.43 ± 0.05	0.44 ± 0.05	0.23 ± 0.03
<i>CAL</i>	f.h.b.c.	0.19 ± 0.03	0.17 ± 0.03	0.15 ± 0.03
	p.b.c.	0.24 ± 0.03	0.26 ± 0.03	0.26 ± 0.03
<i>DD</i>	f.p.b.c.	0.28 ± 0.04	0.26 ± 0.04	0.31 ± 0.04
	p.b.c.	0.18 ± 0.03	0.16 ± 0.03	0.10 ± 0.02
<i>M</i>	f.p.b.c.	0.01 ± 0.01	0.01 ± 0.01	0.03 ± 0.01
	p.b.c.	0.04 ± 0.02	0.03 ± 0.01	0.10 ± 0.02
trivial vacuum	f.p.b.c.	0.06 ± 0.02	0.04 ± 0.02	0.06 ± 0.02
	p.b.c.	0.11 ± 0.02	0.11 ± 0.02	0.31 ± 0.04

This has well-established a new class of semiclassical topological objects that can be “frozen out” from Monte Carlo field configurations

Our paper about calorons and dyons :

- On the topological content of SU(2) gauge fields below T_c , E.-M. I. (Osaka U. RCNP), B. V. Martemyanov (Moscow ITEP), M. Müller-Preussker, S. Shcheredin (Humboldt U. Berlin), A. I. Veselov (Moscow ITEP), Phys. Rev. D66 (2002) 074503

A lot of correspondence with D. Diakonov (St. Petersburg) followed

→ Diakonov's review

- Instantons at work, D. Diakonov, Prog. Part. Nucl. Phys. 51 (2003) 173-222

has fundamentally changed between v2 and v3 (18 Feb 2003):

a third section was added “Non-instanton semiclassical configurations”

Question: Why dyons haven't been seen earlier ?

Non-staticity in dependence on T (changing N_τ at fixed $\beta = 2.2$)

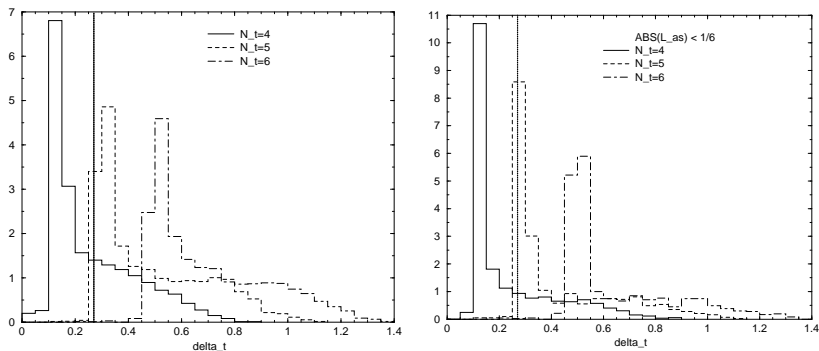


Figure: The distribution of non-staticity δ_τ after cooling as histograms (with bin width 0.05), for three temperatures below deconfinement at $N_\tau = 4$, $N_\tau = 5$ and $N_\tau = 6$: left: without any cut, right: when a cut $|L_{as}| < 1/6$ is applied. The thick vertical line marks the non-staticity $\delta_\tau^* = 0.27$ where the caloron recombines.

Caloron “recombination”

This effect has been studied in

- Recombination of dyons into calorons in SU(2) lattice fields at low temperatures,
E.-M. I. (Humboldt U. Berlin), B. V. Martemyanov (Moscow ITEP),
M. Müller-Preussker (Humboldt U. Berlin), A. I. Veselov (Moscow ITEP),
Phys. Rev. D69 (2004) 114505

Hypothesis :

Most of the “instantons” found by cooling in the confinement phase are actually non-trivial holonomy objects, not dissociated into dyons.

Outline

- 1 Introduction: Cooling and vacuum structure
- 2 Conditions for “freeze-out” of numerical solutions for SU(2)
- 3 Analytical caloron and dyon solutions (for arbitrary SU(N))**
- 4 Conditions for “freeze-out” of SU(3) calorons and dyons
- 5 Why calorons ? Can calorons generate confinement ?
- 6 Overlap analysis of dyon structure in gluodynamics below/above T_{dec}
- 7 Overlap analysis of dyon structure in dynamical QCD at/above T_{χ}
- 8 Outlook and Plans

Generalities on calorons (following van Baal)

A simple formula for a **charge-one** $SU(N)$ caloron action density (= \pm topological density) derived from a potential ψ :

$$\text{Tr } F_{\alpha\beta}^2(x) = \partial_\alpha^2 \partial_\beta^2 \log \psi(x), \quad \psi(x) = \frac{1}{2} \text{tr}(\mathcal{A}_N \cdots \mathcal{A}_1) - \cos(2\pi t).$$

With index $m = 1, \dots, N$ **numbering the constituents**, the 2×2 matrices \mathcal{A}_m are

$$\mathcal{A}_m = \frac{1}{r_m} \begin{pmatrix} r_m & |\vec{\rho}_{m+1}| \\ 0 & r_{m+1} \end{pmatrix} \times \begin{pmatrix} c_m & s_m \\ s_m & c_m \end{pmatrix},$$

with $c_n = \cosh(2\pi\nu_m r_m)$ and $s_n = \sinh(2\pi\nu_m r_m)$, expressed through **distances from \vec{x} to centers \vec{y}_m** or **between subsequent centers \vec{y}_m**

$$r_m = |\vec{x} - \vec{y}_m|, \quad \vec{\rho}_m = \vec{y}_m - \vec{y}_{m-1}$$

taking $b = 1/T = 1$ as basic length scale.

Parameters of the caloron solution

N positions in 3D (approximately those of constituent monopoles) :

$$\vec{y}_1, \vec{y}_2, \dots, \vec{y}_N$$

Asymptotic holonomy (untraced Polyakov loop) :

$$\mathcal{P}_\infty = \text{diag} \left(e^{2\pi i \mu_m} \right), \quad \sum_{m=1}^N \mu_m = 0$$

given in forms of eigenphases, ordered as

$$\mu_1 < \mu_2 < \dots < \mu_N < \mu_{N+1} \equiv 1 + \mu_1,$$

They are determining how action (and topological charge) is fractionally distributed among the lumps:

$$S_m = \nu_m S_{inst} \quad \text{with} \quad \nu_m = \mu_m - \mu_{m-1}.$$

Chiral fermion zero-mode

It must be there, according to **index theorem**, and can be endowed with a **a-periodicity** to be varied freely :

$$\Psi_\phi(t + 1/T, \vec{x}) = e^{-2\pi i\phi} \Psi_\phi(t, \vec{x}).$$

Jumping and **(breathing) of zero-mode** : sectors determined by μ_i

for $\phi \in [\mu_m, \mu_{m+1}] \Rightarrow |\Psi_\phi(x)|^2$ localized at \vec{y}_m
 when $\phi \rightarrow \mu_m \Rightarrow |\Psi_\phi(x)|^2$ becomes delocalized

A specific feature of **Neuberger overlap fermions** : make possible that

- Zero modes are clearly identified, with chirality $= \pm 1$
- **The index theorem is trivially fulfilled: $N_{zm} = |Q_{top}|$**
- Further (paired) topological objects must give rise to pairs of **non-chiral near-zero modes ($N_{nzm} \neq 0$)** that become clearly separable at $T > T_c$ (see later).

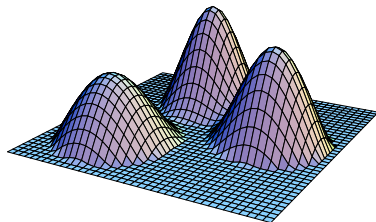
A non-maximally non-trivial caloron for $SU(3)$ 

Figure: Logarithmic plot of the action density of a $SU(3)$ caloron with non-maximally non-trivial holonomy (from van Baal)

SU(3) calorons with nontrivial and trivial holonomy

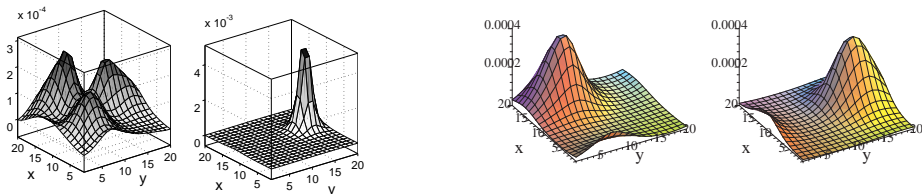


Figure: Left: The topological charge density in the plane through all 3 constituents for nontrivial and trivial holonomy. Right: The scalar density $|\psi|^2$ for the nontrivial caloron looked at with two different boundary conditions.

- Calorons in SU(3) lattice gauge theory,
E.-M. I., M. Müller-Preussker, D. Peschka (Humboldt U. Berlin),
Phys. Rev. D71 (2005) 116003

Global Polyakov loop plots for SU(2) and SU(3)

- The local maxima of $|L(\vec{x})|$ are at the location of the dyons (constituents), at maximal distance from the asymptotic value (asymptotic holonomy).
- For SU(2) the local Polyakov loop $L(\vec{x})$ is real number interpolating between -1 and $+$.
- For SU(3) the Polyakov loop $L(\vec{x})$ is complex-valued.
- Visualization of asymptotic holonomy and local holonomy are provided now in the Weyl-plane !
- Localization of dyons(=monopoles) by degenerate eigenvalues of local holonomy (populating the periphery of the Weyl plot).

Schematic Weyl plots for an SU(3) caloron

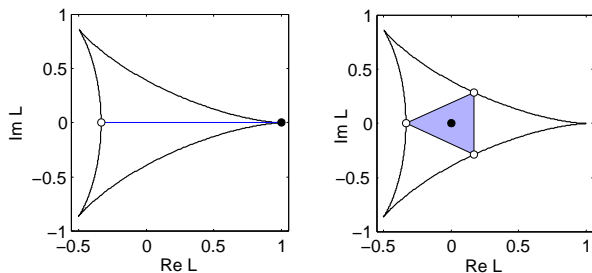


Figure: Schematic scatterplots in the complex plane (left: on the real axis, right: inside the Weyl plot) of the local Polyakov loop values $L(\vec{x})$, for a $SU(3)$ caloron with trivial holonomy $L_\infty = +1$ (left) and with maximally non-trivial holonomy $L_\infty = 0$ (right). Black dots indicate the asymptotic Polyakov loop values, whereas white circles on the boundary give the local Polyakov loop values at the monopole constituents according to two eigenvalues of \mathcal{P} becoming degenerate.

Realistic Weyl plot for a non-trivial SU(3) caloron

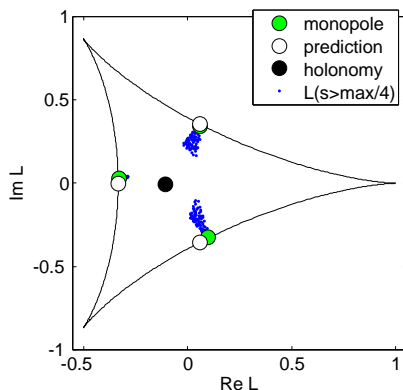


Figure: Realistic scatterplot of a not maximally non-trivial caloron by plotting of lattice points in the Weyl plane according to their local action density.

Localization by monopoles in the Maximal Abelian Gauge for $SU(2)$ and $SU(3)$

- The Monopole content of topological clusters: Have KvB calorons been found ?
E.-M. I. (Humboldt U. Berlin), B. V. Martemyanov (Moscow ITEP), M. Müller-Preussker (Humboldt U. Berlin), A. I. Veselov (Moscow ITEP), Phys. Rev. D71 (2005) 034505
- Calorons and monopoles from smeared $SU(2)$ lattice fields at non-zero temperature,
E.-M. I. (Humboldt U. Berlin), B. V. Martemyanov (Moscow ITEP), M. Müller-Preussker (Humboldt U. Berlin), A. I. Veselov (Moscow ITEP), Phys. Rev. D73 (2006) 094509
- Calorons in $SU(3)$ lattice gauge theory,
E.-M. I., M. Müller-Preussker, D. Peschka (Humboldt U. Berlin), Phys. Rev. D71 (2005) 116003

Localization by Abelian monopole fields in the Maximal Abelian Gauge for $SU(3)$

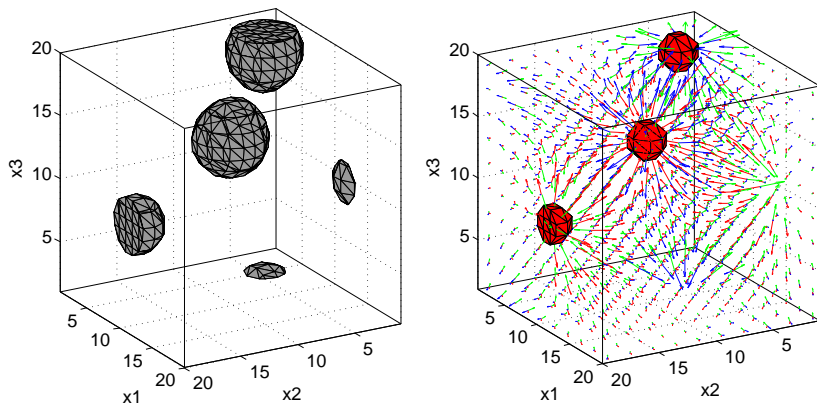


Figure: An $SU(3)$ caloron. Left: three lumps of action showing well-separated (static) dyons. Right: three Abelian electric (equal to - magnetic) field strengths in the Maximal Abelian Gauge. The surfaces are isosurfaces of the Abelian action close to the dyon positions.

Localization by monopoles which are defined by minimal distance between holonomy eigenvalues

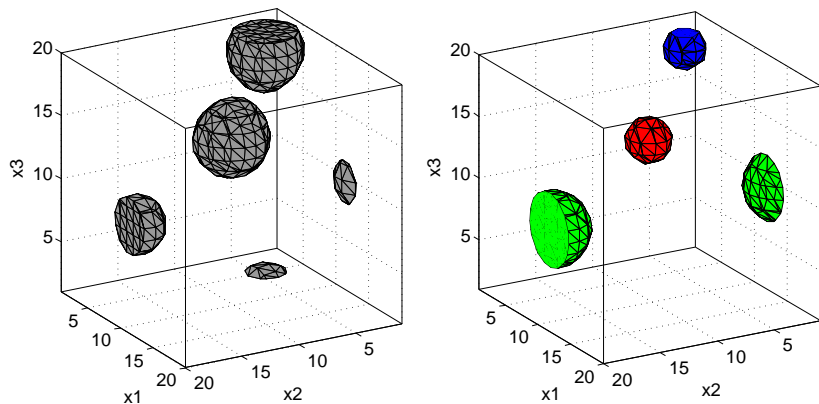


Figure: An SU(3) caloron. Left: three lumps of action showing well-separated (static) dyons. Right: Monopoles localized by isosurfaces of the minimal distance between two eigenvalues of the holonomy $f(\vec{x}) = \min_{i,j} |e^{i\phi_i(\vec{x})} - e^{i\phi_j(\vec{x})}|$.

Modulation of the lowest Dirac eigenmodes by changing BC

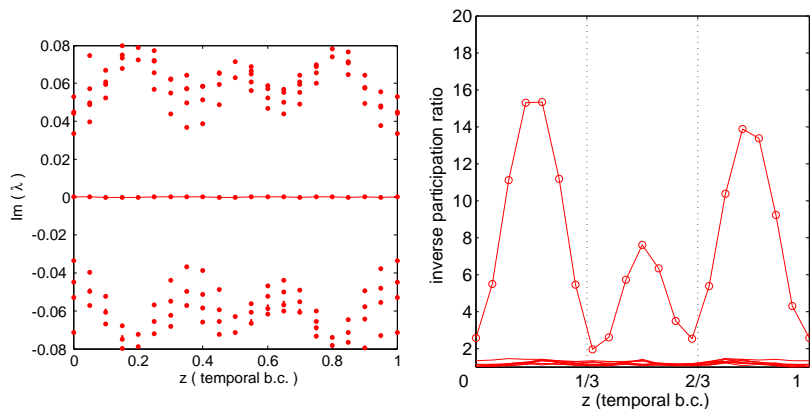


Figure: An SU(3) caloron. Left: the band of lowest modes modulated by changing temporal boundary conditions. Right: the inverse participation ratio only of the zero mode changes by changing temporal boundary conditions. Three maxima of the “gap”, three maxima of IPR.

Localization of dyons and antidyons in a configuration with $S = 2S_{\text{inst}}$ and $Q_{\text{top}} = 0$

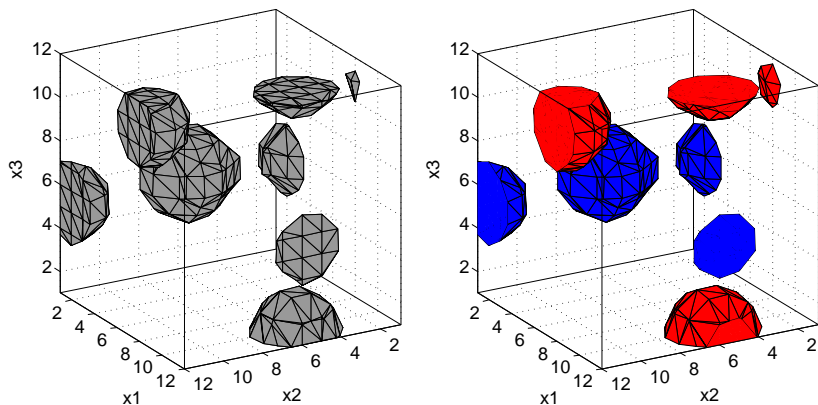


Figure: Two dyon-antidyon pairs. Left: four lumps of action showing well-separated (static) dyons/antidyons. Right: topological charge (red=positive, blue=negative).

Outline

- 1 Introduction: Cooling and vacuum structure
- 2 Conditions for “freeze-out” of numerical solutions for SU(2)
- 3 Analytical caloron and dyon solutions (for arbitrary SU(N))
- 4 Conditions for “freeze-out” of SU(3) calorons and dyons**
- 5 Why calorons ? Can calorons generate confinement ?
- 6 Overlap analysis of dyon structure in gluodynamics below/above T_{dec}
- 7 Overlap analysis of dyon structure in dynamical QCD at/above T_{χ}
- 8 Outlook and Plans

Lattice set-up for caloron and dyon discovery in SU(3)

Start from Monte Carlo ensembles thermalized with Wilson action at $\beta = 5.65$.

For $N_\tau = 4$ and $N_\tau = 6$ this corresponds to $T/T_{\text{dec}} \approx 0.91$ and 0.6 .

Various lattice sizes have been chosen for Wilson cooling :

- $4 \times 12^3, 6 \times 12^3, 4 \times 30^3, 6 \times 20^3$ for $T \neq 0$
- 12^4 for $T = 0$

Monitoring is done :

- by non-staticity δ_t
- violation of (anti)selfduality
(Notice : There are no strict $Q_{\text{top}} = \pm 1$ solutions on a torus !)

Results for SU(3)

Tools had been considerably improved since 2002 :

- $\mathcal{O}(a^4)$ improved field strength tensor via clover definition of $F_{\mu\nu}(x)$
- Clover-improved Wilson-Dirac operator by adding the clover term

$$D_{x,y} = D_{x,y} + \frac{i}{2}\kappa c_{sw} \sigma_{\mu\nu} F_{\mu\nu}(x) \delta_{x,y}$$

Aim: High precision measurement of topological charge and spectrum should now be possible !

Results :

- On 4×12^3 we found multiply topologically charged configurations up to $|Q_{\text{top}}| = 6$, on 6×12^3 up to $|Q_{\text{top}}| = 7$, and on 12^4 up to $|Q_{\text{top}}| = 10$.
- Detailed study of these ensembles.
- Perfectly 3 constituents per unit of Q_{top} visible up to $|Q_{\text{top}}| = 4$.

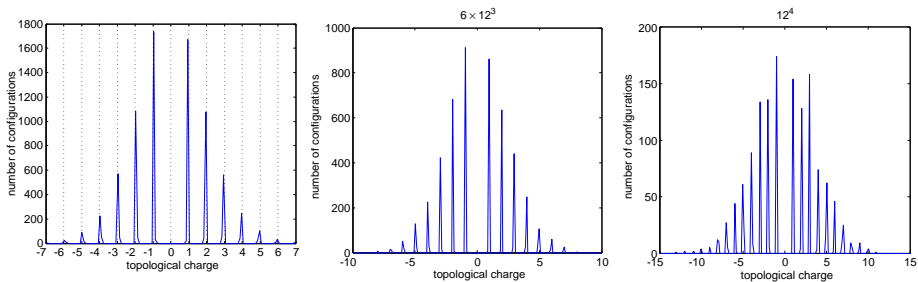
Results for SU(3) : Q_{top} -histograms

Figure: The Q_{top} -histograms (apart from $Q_{\text{top}} = 0$) for 4×10^3 (left), 6×10^3 (center) and 12^4 (right).

Results for SU(3) : “non-staticity”

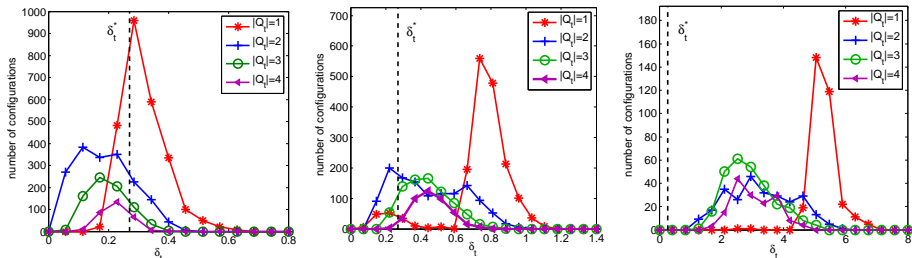


Figure: Left: histograms of non-staticity for 4×12 separated w.r.t. $|Q_{\text{top}}|$. Center: the same for 6×12^3 . Right: the same for the 12^4 torus.

Non-staticity moves to large values with lowering of temperature.

$Q_{\text{top}} = \pm 1$ configurations always special !

Results for SU(3) : Quality of selfduality

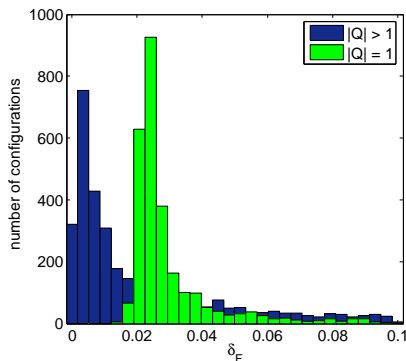


Figure: Histograms of "violation of (anti) selfduality" separated with respect to $|Q_{\text{top}}|$.

Outline

- 1 Introduction: Cooling and vacuum structure
- 2 Conditions for “freeze-out” of numerical solutions for SU(2)
- 3 Analytical caloron and dyon solutions (for arbitrary SU(N))
- 4 Conditions for “freeze-out” of SU(3) calorons and dyons
- 5 Why calorons ? Can calorons generate confinement ?**
- 6 Overlap analysis of dyon structure in gluodynamics below/above T_{dec}
- 7 Overlap analysis of dyon structure in dynamical QCD at/above T_{χ}
- 8 Outlook and Plans

Simulating a caloron-anticaloron gas for SU(2)

First step: studies of the first steps towards confinement employing the additional caloron degrees of freedom.

- **Approximative superposition scheme** (like instanton simulations).
- This requires calorons and anticalorons of **equal holonomy**, **added in the algebraic gauge**.
- **Global gauge trafo** of the sum ansatz **into the periodic gauge**.
- **Discretization of space-time** into $32^3 \times 8$ lattice.
- **Discretization of the gauge field** by mapping to lattice links.
- **Interaction between Dirac strings inside separate calorons can be neglected** as long as calorons are not too large ! (improved ansatz in the separate paper B)
- **Action excess parameter** $\gamma = S(\sum_n A^n) / \sum_n S(A^n)$ **to control diluteness** (reliability of the ansatz).

Superpositions for higher density n and larger ρ ?

- Improved superposition schemes for approximate multi-caloron configurations,
Ph. Gerhold, E.-M. I., M. Müller-Preussker (Humboldt U. Berlin),
Nucl. Phys. B774 (2007) 268-297

Two complications, two new techniques :

- Dealing with the “Dirac strings” between constituents; (actually an Abelian Dirac string only in the limit $\rho \rightarrow \infty$)
Question “How constituents of another caloron interact with the Dirac string of another ?”
- Dealing with constituents coming close; ADHM construction offers method how to improve the (anti)selfduality.

The second method is close in spirit to Edward Shuryak's ratio ansatz.

Parameters of the SU(2) caloron-anticaloron gas

- An SU(2) KvBLL caloron gas model and confinement, P. Gerhold, E.-M. I., M. Müller-Preussker, Nucl. Phys. B760 (2007) 1
- Holonomy (uniform quantity, entering via calorons/anticalorons), described by ω , extreme cases: $\omega = 0$ (trivial, HS caloron) and $\omega = 0.25$ (maximally nontrivial). **Holonomy = crucial parameter.**
- Inverse temperature $\beta = 1/T = 1 \text{ fm}$ by default.
- Caloron and anticaloron density $n = 1 \text{ fm}^{-4}$ by default.
- Caloron size parameter fixed (to $\rho = 0.33 \text{ fm}$) or fluctuating.
- caloron field \rightarrow anticaloron field

$$A_j^{\text{anti}}(\vec{x}, t) = -A_j^{\text{cal}}(-\vec{x}) \qquad A_4^{\text{anti}}(\vec{x}) = A_4^{\text{cal}}(-\vec{x})$$

Role of the holonomy parameter on confinement and the spatial string tension

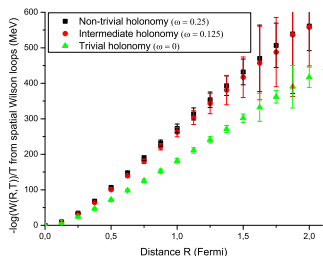
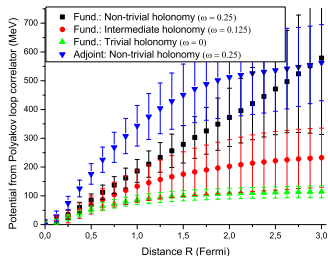


Figure: Left: The potential for fundamental and adjoint static charges from the corresponding Polyakov loop correlators. Right: linearly rising “potential” for fundamental charges from spatial Wilson loops. Note the different asymptotic holonomies ω .

Casimir scaling and T -dependent holonomy

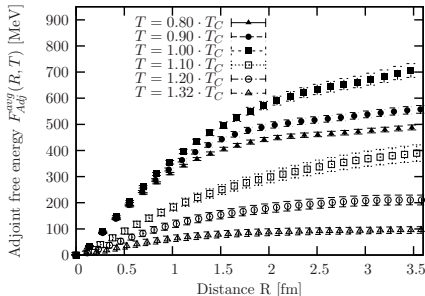
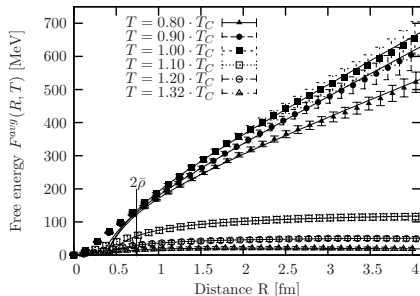


Figure: Colour averaged free energy versus distance R at various temperatures for the fundamental (left) and adjoint (right) representations.

Area law and Casimir scaling for spacelike Wilson loops

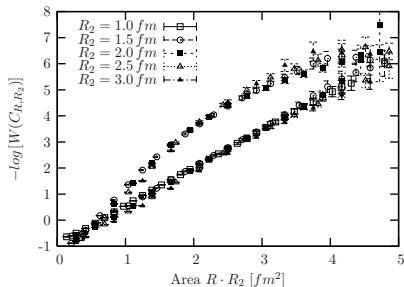


Figure: Negative logarithm of rectangular Wilson loops, $-\log(W(C_{R,R_2}))$, with side lengths R and R_2 in fundamental (lower curve) and adjoint representation (upper curve) versus the area $A = R \cdot R_2$. The different symbols correspond to different side lengths R_2 .

Parametrization by $L_{\text{ren}}(T)$ and $\chi_{\text{top}}(T)$

T	$L_{\text{ren}}(T)$	$4\omega(T)$	$n(T) = \chi_{\text{top}}(T)$
$\leq T_c$	0.0	1.0	$(198 \text{ MeV})^4$
$1.10 T_c$	0.58	0.61	$(178 \text{ MeV})^4$
$1.20 T_c$	0.70	0.51	$(174 \text{ MeV})^4$
$1.32 T_c$	0.78	0.43	$(165 \text{ MeV})^4$
$1.54 T_c$	0.85	0.35	$(157 \text{ MeV})^4$
$1.79 T_c$	1.0	0.00	$(136 \text{ MeV})^4$

Table: Values of the renormalized Polyakov loop as obtained by Digal et al. (2003). The holonomy parameter $\omega(T)$ for the caloron gas model is fixed (up to the $Z(2)$ symmetry between ω and $\bar{\omega}$) by the dilute gas relation $L_{\text{ren}}(T) = \cos(2\pi\omega)$. The $SU(2)$ topological susceptibility is taken from Alles et al. (1997).

Size distribution :

$$D(\rho, T < T_c) = A\rho^{b-5} e^{-c\rho^2} \quad D(\rho, T > T_c) = B\rho^{b-5} e^{-\frac{4}{3}(\pi\rho T)^2 G(\omega)}$$

$$G(\omega) = 16 C_0(\omega) \pi^2 \omega^2 \bar{\omega}^2 + 4 (\omega^2 + \bar{\omega}^2 - 4 \omega \bar{\omega})$$

trivial holonomy \rightarrow D. Gross, R. Pisarski, L. Yaffe, RMP 53, 43 (1981)

Outline

- 1 Introduction: Cooling and vacuum structure
- 2 Conditions for “freeze-out” of numerical solutions for SU(2)
- 3 Analytical caloron and dyon solutions (for arbitrary SU(N))
- 4 Conditions for “freeze-out” of SU(3) calorons and dyons
- 5 Why calorons ? Can calorons generate confinement ?
- 6 Overlap analysis of dyon structure in gluodynamics below/above T_{dec}**
- 7 Overlap analysis of dyon structure in dynamical QCD at/above T_{χ}
- 8 Outlook and Plans

Fermionic definition of topological density, depending on boundary conditions : ambiguity or virtue ?

This technique has been applied in the years 2007–2009 to $SU(2)$ Yang-Mills theory at the thermal phase transition and in deconfinement

- V. G. Bornyakov, E.-M. I., B. V. Martemyanov, S. M. Morozov, M. Müller-Preussker and A. I. Veselov
Phys. Rev. D76 (2007) 054505, Phys. Rev. D77 (2008) 074507,
Phys. Rev. D79 (2009) 034506
(arXiv: 0706.4206, 0708.3335, 0809.2142)

Recently (2013–2015) : the overlap fermionic method of dyon search was extended to $SU(3)$ (YM and QCD) with new features:

three types of dyons, complex patterns of the Polyakov loop.

- V. G. Bornyakov, E.-M. I., B. V. Martemyanov, M. Müller-Preussker
Phys. Rev. D89 (2014) 054503, Phys. Rev. D91 (2015) 074505,
Phys. Rev. D93 (2016) 074508
(arXiv:1309.7850, 1410.4632, 1512.03217)

A selective view on topological density

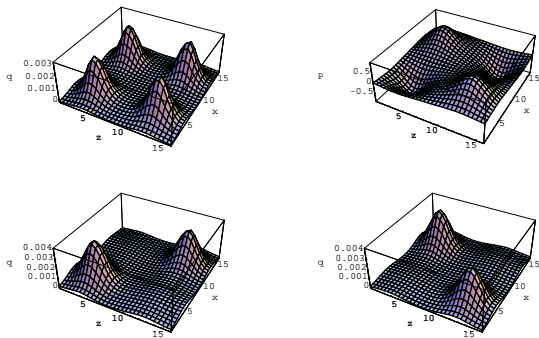


Figure: **Top:** The gluonic topological charge density $q_{\text{gluon}}(x)$ (left) and the Polyakov loop $p(\vec{x})$ (right) for a classical $Q = 2$ configuration generated at maximally nontrivial holonomy (asymptotically $p(\vec{x}) = 0$) on a $16^3 * 4$ lattice (with four dyons maximally separated in the (x, z) -plane). **Bottom:** The fermionic topological charge density $q^{(p/a)}(x)$ reconstructed out of the 20 lowest eigenmodes of the overlap Dirac operator with periodic (right) and antiperiodic (left) temporal boundary conditions.

Calorons or dyons in case of SU(2) ?

$P(x)$ and $q(x)$ real-valued: four quadrants

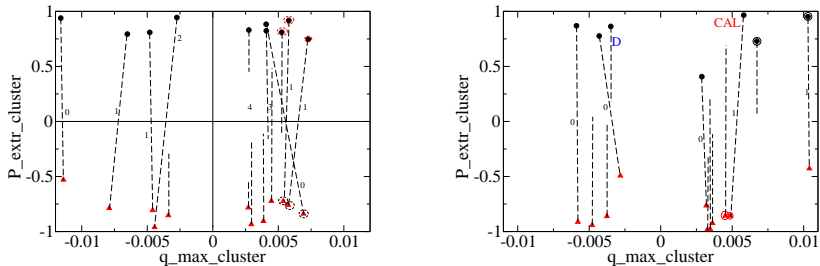


Figure: The maxima of clusters of the fermionic $|q(x)|$ seen under periodic boundary condition (filled circles) and under antiperiodic boundary condition (filled triangles) for two configurations in the ensemble, shown in the $q_{max_cluster}$ - $P_{extr_cluster}$ plane. Peaks at opposite-sign of $P_{extr_cluster}$, that are connected by dashed lines, have appeared under different boundary conditions at the same space-time position ("not jumping") and are interpreted as calorons. Isolated peaks have appeared only once under the respective boundary condition at the given position ("jumping") and are interpreted as dyons. The marked objects "D" and "CAL" in the bottom plot are portrayed in detail in the next figure.

A single caloron and a single dyon

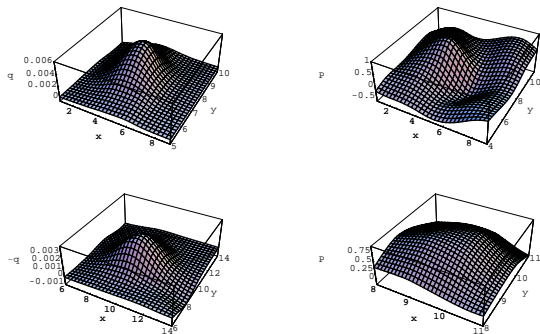


Figure: The fermionic topological charge density $q^{(p/a)}(x)$ (left) and the Polyakov loop $p(\vec{x})$ (right). The upper row shows a typical caloron cluster (when $q^{(p)}(x) \approx q^{(a)}(x)$) and the lower row shows a typical single-dyon cluster (which was visible only with periodic boundary conditions, in $q^{(p)}(x)$). The topological density and the Polyakov loop are represented as function over an appropriate part of the (x, y) -plane. Notice the difference in scales for the topological charge density and for the Polyakov loop between the two solutions. The Polyakov loop is measured after $N_{\text{APE}} = 10$ smearing steps.

Typical for the high temperature phase: dyon-antidyon pair, visible or invisible (due to BC)

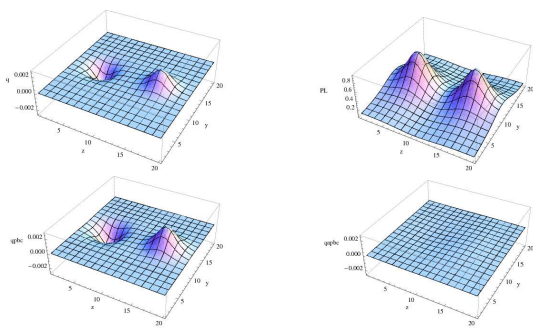


Figure: **Top:** The gluonic topological charge density $q_{\text{gluon}}(x)$ (left) and the Polyakov loop $p(\vec{x})$ (right) for a $Q = 0$ configuration containing a dyon-antidyon pair at not maximally nontrivial holonomy (asymptotically $p(\vec{x}) \neq 0$) on a $16^3 * 4$ lattice. **Bottom:** The fermionic topological charge density $q^{(P/A)}(x)$ reconstructed out of the 20 lowest eigenmodes of the overlap Dirac operator with periodic (left) and antiperiodic (right) temporal boundary. The pair is "invisible" for antiperiodic boundary conditions.

The corresponding Dirac spectrum

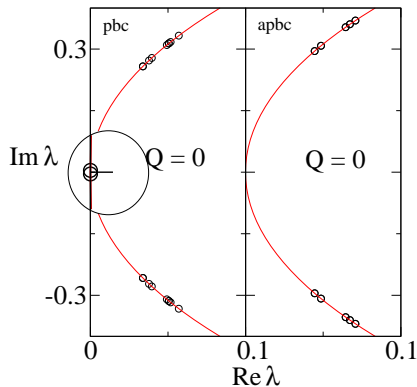


Figure: Dirac spectrum for periodic (left) and antiperiodic (right) boundary condition.

A systematic study of the topological structure

Using overlap fermions gives the opportunity for a “non-destructive” topological investigation of gauge field configurations.

Two “subjective” factors are welcome :

- **number of included pairs of NZM or λ cutoff** (defines resolution),
- **boundary conditions** select dyons according to local holonomy.

For diagonalization of the overlap Dirac operator (using ARPACK) this means :

- **processing each configuration 2-times for SU(2)**
(only periodic/antiperiodic boundary conditions)
- **processing each configuration 3-times for SU(3)**
(here, three angles at least)

The **BC influence the whole band of NZM** \rightarrow details of the topological charge distribution, beyond the chiral zero mode (which is only present if $Q_{\text{top}} \neq 0$). Therefore, also the $Q_{\text{top}} = 0$ configurations show different topological views for different BC.

What shall we look for ? Differences between the phases ...

- Clustering of the topological charge distribution, different for all chosen BC.
- Statistical properties of all sorts of clusters at temperatures near T_{dec} and above.
- Localization properties for each sort of clusters at low and high temperature.
- Finally : Comparison of topological clusters and monopoles as defined in Maximal Abelian gauge at higher temperature.

Set-up to generate smooth configurations representing quenched LGT

- lattice of size $20^3 \times 6$
- pure $SU(3)$ gauge theory
- **Lüscher-Weisz action instead of Wilson action**
- robust overlap spectrum requires smooth configurations: criterion, that **change of the boundary condition leaves the index (number of zero modes) unchanged**
- Two ensembles (each 50 configurations) for the overlap analysis generated at $\beta = 8.20$ and $\beta = 8.25$
- **warning: at essentially lower β (deeper in confinement phase) the reproducibility of the index would be lost even for LW action !**

Lüscher-Weisz action

$$S[U] = \beta \left(\sum_{pl} \frac{1}{3} \text{Re Tr}[1 - U_{pl}] \right. \\ \left. + c_1 \sum_{rt} \frac{1}{3} \text{Re Tr}[1 - U_{rt}] \right. \\ \left. + c_2 \sum_{pg} \frac{1}{3} \text{Re Tr}[1 - U_{pg}] \right),$$

β is the principal inverse coupling parameter.

c_1 and c_2 are from one-loop perturbation theory and tadpole improvement:

$$c_1 = -\frac{1}{20u_0^2} [1 + 0.4805\alpha], \quad c_2 = -\frac{1}{u_0^2} 0.03325\alpha.$$

Tadpole and one-loop improvement

For any β , the tadpole factor u_0 and the lattice coupling constant α are self-consistently determined in terms of the average plaquette

$$u_0 = \left(\left\langle \frac{1}{3} \text{Re Tr } U_{pl} \right\rangle \right)^{1/4}, \quad \alpha = - \frac{\ln \left(\left\langle \frac{1}{3} \text{Re Tr } U_{pl} \right\rangle \right)}{3.06839}$$

by an iterative search.

Comparison of Polyakov loop distributions

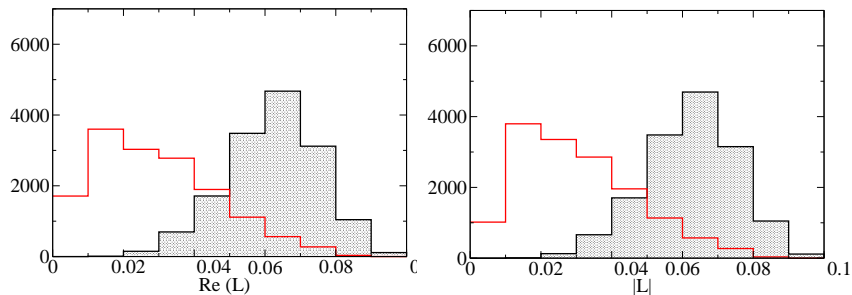


Figure: Distribution of the real part $\Re L$ (left) of the spatially averaged Polyakov loop L and of the modulus $|L|$ (right) at $\beta = 8.20$ (curve) and $\beta = 8.25$ (shaded). If necessary, a $Z(3)$ flip towards the real sector has been applied.

Comparison of the two ensembles

This confirms :

- $\beta = 8.20$ belongs mainly to the confining phase (admixture of deconfinement to be eliminated, eventually by Polyakov loop cuts).
- $\beta = 8.25$ exclusively belongs to the deconfining phase.

One might suppose :

- Polyakov loop distributions at $\beta = 8.20$ and $\beta = 8.25$ are sufficiently different (taken as “asymptotic holonomy”) therefore able to produce noticeable differences between dyons.

However :

- The Polyakov loop modulus $|\overline{L}|$ on the “deconfined side” is numerical still too small to expect the full effect of the Polyakov loop on the statistical weight of different dyons.

Overlap Dirac operator

The **Neuberger operator** is a solution of the **Ginsparg-Wilson relation**

$$D\gamma_5 + \gamma_5 D = \frac{a}{\rho} D\gamma_5 D ,$$

As the **input kernel** we take the **Wilson-Dirac operator**; the solution is

$$D_{\text{ov}} = \frac{\rho}{a} \left(1 + D_W / \sqrt{D_W^\dagger D_W} \right) , \quad D_W = M - \frac{\rho}{a} .$$

D_W is the Wilson-Dirac operator with a negative mass term ρ/a , M is the Wilson hopping term with $r = 1$.

An optimal choice is $\rho \approx 1.4$.

For the **sign function** in the alternative expression

$$D_W / \sqrt{D_W^\dagger D_W} = \gamma_5 \operatorname{sgn}(H_W) , \quad H_W = \gamma_5 D_W ,$$

the minmax polynomial approximation (Giusti 2002) was used.

Fermionic topological charge density

The **Pontryagin density** can be expressed in the form

$$q(x) = -\text{tr} \left[\gamma_5 \left(1 - \frac{a}{2\rho} D_{\text{ov}}(x, x) \right) \right].$$

tr is the trace only over color and spinor indices.

This topological charge density contains vacuum fluctuations of all scales.

An **ultraviolet filtered (mode-truncated) density** is

$$q_{\lambda_{\text{cut}}}(x) = - \sum_{|\lambda| \leq \lambda_{\text{cut}}} \left(1 - \frac{\lambda}{2} \right) \psi_{\lambda}^{\dagger}(x) \gamma_5 \psi_{\lambda}(x)$$

and shows **conventional clustering of topological charge**

(instanton-like, decomposed into dyons = “instanton quarks” ?)

which **resembles the effect of smearing/cooling** without doing cooling.

Modified boundary conditions and Dirac spectrum

For the improved action in the β range under investigation, the index is unchanged and the spectrum approximately unchanged under a change of boundary conditions.

In $SU(2)$ we used antiperiodic and periodic boundary conditions to map out clusters of topological charge with the required sign of the local Polyakov loop (holonomy).

Here, for $SU(3)$ we selected three angles for use in the boundary conditions:

two complex BC, and the (physical) antiperiodic BC.

$$\psi(1/T) = \exp(i\phi)\psi(0)$$

with

$$\phi = \begin{cases} \phi_1 \equiv -\pi/3, \\ \phi_2 \equiv +\pi/3, \\ \phi_3 \equiv \pi. \end{cases}$$

Where does the Dirac spectrum start to depend on boundary conditions ? This dependence sets in at T_{dec} .

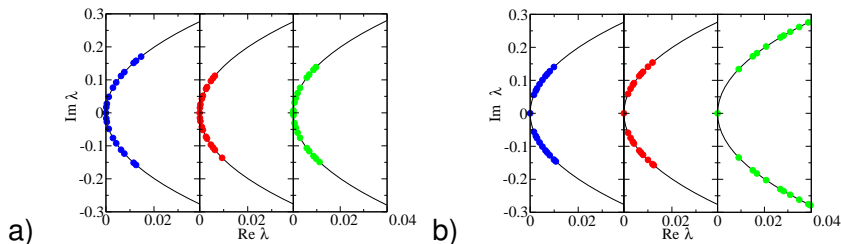


Figure: For two typical configurations and in each case for the three versions of the fermion temporal b.c. the 20 lowest eigenvalues of the $SU(3)$ overlap Dirac operator are shown, for a) $\beta = 8.20$ and b) $\beta = 8.25$, respectively. In both of the panels for $\phi = \phi_1$ the spectrum is shown left (in blue), for $\phi = \phi_2$ in the middle (in red), and for $\phi = \phi_3$ (antiperiodic b.c.) it is plotted right (in green), respectively.

Three (selective) topological densities instead of one unique (gluonic one)

We have reconstructed from the zero and the non-zero modes the profiles of the UV-filtered topological charge density, **detailed for the three boundary conditions**, according to its spectral representation

$$q_{i,N}(x) = - \sum_{j=1}^N \left(1 - \frac{\lambda_{i,j}}{2} \right) \psi_{i,j}^\dagger(x) \gamma_5 \psi_{i,j}(x),$$

where j enumerates the eigenvalues $\lambda_{i,j}$ equal and closest to zero. These eigenvalues $\lambda_{i,j}$, as well as the corresponding modes $\psi_{i,j}(x)$, are also characterized by the i -th boundary condition.

Correspondingly, the UV-filtered topological density $q_{i,N}(x)$ depends on the boundary condition, too.

Cluster analysis made for all three charge densities

Cluster analysis with a variable lower cut-off $q_{\text{cut}} > 0$:

- first step: the algorithm identifies the interior of all clusters (“topological cluster matter”) as the region where $|q(x)| > q_{\text{cut}}$.
- crucial next step: enquire **connectedness** between the lattice points in order to form **individual clusters out of this “cluster matter”**.

Neighbouring points with $|q(x)|$ above threshold and sharing the sign of topological density belong to the same cluster.

- choice of the cut-off q_{cut} : made such as to decompose the “continuous” distribution into a maximal number of **internally connected clusters**, being mutually separated (q_{cut} is independently adapted for each configuration).

The purpose of the cluster analysis was to discover **extended objects as dyon candidates of different kind** in order to study their “space-time coordination” and Polyakov line profiles, similar to the SU(2) case.

Later, well above the deconfinement transition, also their relation to the **Maximal Abelian gauge monopoles** has been investigated.

Then, we will try to find that the **heavy dyons** (found with antiperiodic boundary conditions) are in **one-to-one relation to Abelian thermal monopoles** at $T = 1.5 T_{\text{dec}}$. The correlation is however weaker than expected.

Abundance of the three sorts of clusters

At lower temperature

- For the lower temperature ($\beta = 8.20$) we have found the following average numbers of clusters per configuration :

$$N_1 = 18.4(0.4), \quad N_2 = 18.6(0.5), \quad N_3 = 16.6(0.3).$$

- The nomenclature corresponds to the configuration being rotated if needed (by a $Z(3)$ flip) into the real $Z(3)$ sector (such that the average Polyakov loop has $-\pi/3 < \arg(\bar{L}) < \pi/3$).
- N_1 and N_2 are coinciding within errors, while N_3 is slightly less.
- The average size of all clusters amounts to 146 lattice points.
- However, the abundance of all three types of clusters should be equal for confining configurations.**

(A)symmetry in multiplicity between sorts of dyons ?

- Assuming the lattice scale fixed by the transition temperature for $SU(3)$ gluodynamics ($T_c \approx 300$ MeV) we estimate the physical dyon cluster density: $\rho \approx 6 \text{ fm}^{-4}$.
- The observed slight asymmetry $N_3 < N_1 = N_2$ may be due to the admixture of configurations related to deconfinement.
- We applied a Polyakov cut for the modulus $|\bar{L}| < 0.3$:

$$N_1 = 17.8(0.6), \quad N_2 = 18.3(0.6), \quad N_3 = 17.2(0.5).$$

- The inverse participation ratios (IPR) characterizing the zero modes for three types of b.c.'s are very different :

$$IPR_1 = 6.8(0.8), \quad IPR_2 = 6.4(1.0), \quad IPR_3 = 15.2(1.7),$$

- Having applied the above mentioned cut for $|\bar{L}|$ we find only :

$$IPR_1 = 5.8(0.9), \quad IPR_2 = 5.0(0.6), \quad IPR_3 = 8.5(0.6).$$

Even with this cut, a small asymmetry of multiplicities and IPR remains.

At temperature slightly higher than T_{dec}

Temperature slightly higher:

onset of statistical suppression of “heavy dyons” ?

- Average number of clusters

$$N_1 = 20.7(0.6), \quad N_2 = 20.6(0.6), \quad N_3 = 17.1(0.4)$$

reflecting the different distribution of \bar{L} .

- The asymptotic holonomy would (for an exact caloron) provide the dyon constituents corresponding to antiperiodic fermionic boundary conditions with a higher action.
- Average size of these clusters amounts to 172 lattice points (20 percent larger in lattice units).
- **Density of clusters is higher than at lower temperature :**

$$\rho \approx 8 \text{ fm}^{-4}$$

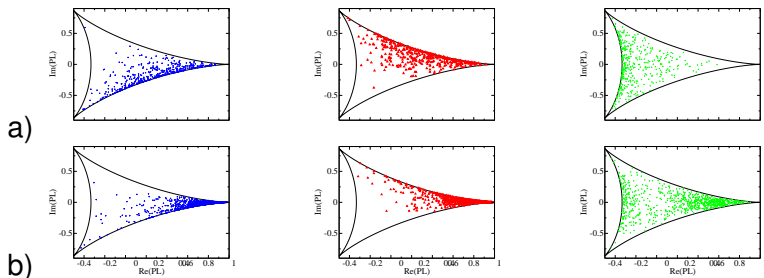


Figure: The clusters defined through the three boundary conditions are located according to their Polyakov loop in the Weyl plot: a) (top) at $\beta = 8.20$ (below T_{dec}): all sorts of clusters concentrated along the sides towards the angle ϕ_j ; b) (bottom) at $\beta = 8.25$ (above T_{dec}): all sorts of clusters populating the trival corner, part of the third sort also populating the negative side.

Localization becomes a clear characteristics of “heavy dyons” at temperature higher than T_{dec}

- Even more pronounced asymmetry is seen in the IPR :

$$IPR_1 = 7.9(0.8), \quad IPR_2 = 7.2(0.7), \quad IPR_3 = 24.6(1.8).$$

For antiperiodic b.c. all low modes are localized about three times more than modes sitting on “light dyons”.

Conclusion : changes go in the expected direction

- “heavy dyons” are more suppressed
- the number density of “dyons” is increased
- light clusters become larger in space-time
- heavy clusters are much (!) more concentrated
- actually heavy dyons are characterized by having “their” local Polyakov loop opposite to trivial $L = 1$?

“Clouds” of topological charge plotted in the Weyl plot

Result :

- Calorons interconnect the three sides ...
- Dyon pairs interconnect two sides ...
- Isolated dyons are located close to the periphery (according to the monopole property) ...

..... of the Weyl plot.

The sides correspond to the three angles ϕ_j .

This result is as expected.

“Clouds” : from single dyons to calorons

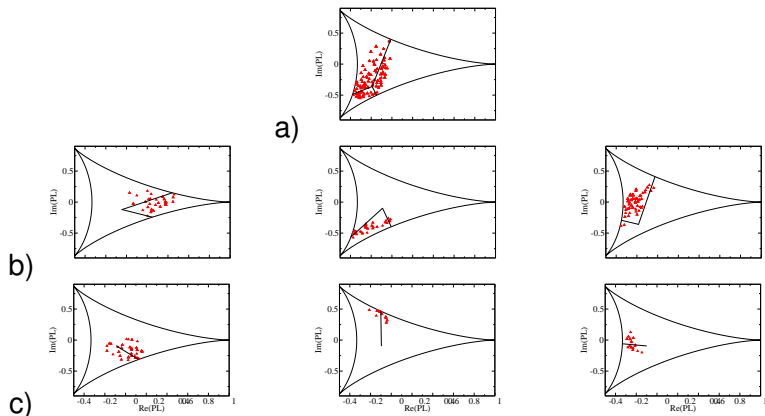


Figure: The profile of the local Polyakov loop L in examples of topological “clouds” formed a) by a triplet of clusters (top), b) by (three types of) cluster pairs (middle) and c) consisting of (three types of) isolated clusters (bottom). This pattern obtained for $\beta = 8.20$ is characteristic for the confining phase. In the figures straight lines are connecting the point representing the averaged Polyakov loop \bar{L} of the cooled configuration and the point (or points) representing the local Polyakov loop $L(\vec{x})$ in the respective dyon center(s).

Inter-cluster correlations

At lower temperature

number of isolated clusters	=	1299	(49%),
number of clusters in pairs	=	782	(29%),
number of clusters in triplets	=	597	(22%),

We see full caloron-like clusters and completely dissolved caloron constituents coexisting in this ensemble.

For the slightly higher temperature

number of isolated clusters	=	1600	(55%),
number of clusters in pairs	=	834	(28%),
number of clusters in triplets	=	492	(17%).

Conclusion : at this temperature the amount of fully dissociated dyons has grown at the expense of dyons enclosed in calorons.

At $T = 1.5T_{\text{dec}}$: heavy dyons weakly correlated with thermal monopoles

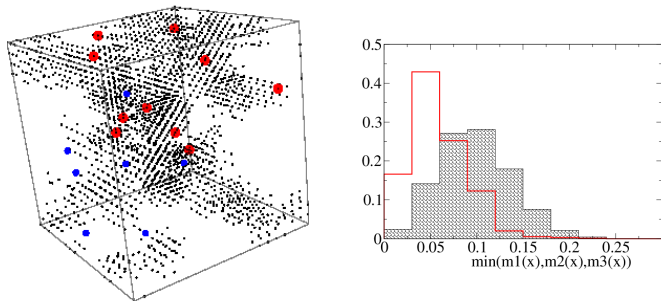


Figure: Left: The location of static time-like monopole loops intersection the 3D projection of topological cluster. Right: The histogram of minimal distance to the Weyl plot boundary: biased for monopoles (open red histogram) compared to all lattice sites.

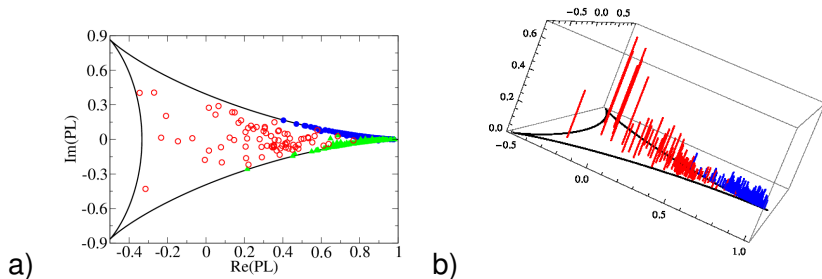


Figure: a) Scatter plots of Polyakov loop PL (after 4 steps of cooling) in clusters selected to contain monopoles. The clusters are separated according to the type of boundary condition for the overlap near-zero modes. For clusters of first type the Polyakov loop is shown by green triangles, for clusters of second type - by blue filled circles, for clusters of third type - by red open circles, b) The maximum of the topological charge density inside the respective cluster is additionally shown in respective color (for second and third type clusters only).

Outline

- 1 Introduction: Cooling and vacuum structure
- 2 Conditions for “freeze-out” of numerical solutions for SU(2)
- 3 Analytical caloron and dyon solutions (for arbitrary SU(N))
- 4 Conditions for “freeze-out” of SU(3) calorons and dyons
- 5 Why calorons ? Can calorons generate confinement ?
- 6 Overlap analysis of dyon structure in gluodynamics below/above T_{dec}
- 7 Overlap analysis of dyon structure in dynamical QCD at/above T_{dec}
- 8 Outlook and Plans

A recent paper

Dyons near the transition temperature in lattice QCD

V. G. Bornyakov (FEFU Vladivostok, ITEP Moscow and IHEP Protvino), E.-M. I. (JINR Dubna),
B. V. Martemyanov (ITEP Moscow, MEPHI Moscow and MIPT Dolgoprudny), M. Müller-Preussker[†] (Humboldt U., Berlin),

Phys. Rev. D93 (2016) 074508 e-Print: arXiv:1512.03217

Set-up to generate the lattice configurations

Configurations left from the DESY-ITEP-Kanazawa (DIK) collaboration.

Gauge field configurations generated with **Wilson gauge action S_W** .
 $N_f = 2$ dynamical flavors of nonperturbatively $O(a)$ improved Wilson fermions (clover fermions).

DESY-ITEP-Kanazawa collaboration has used the “Berlin QCD” code.

The improvement coefficient c_{SW} was determined nonperturbatively.

Scale setting: lattice spacing and pion mass had been determined by interpolation of $T = 0$ results obtained by QCDSF collaboration

$N_\tau = 8$ and $N_s = 16$ (**ensemble I** of 50 configurations at $T = T_\chi$)

$N_\tau = 8$ and $N_s = 24$ (**ensemble II** of 50 configurations at $T = 1.06 T_\chi$)

Cross-over

DIK collaboration: temperature scan made at fixed β by changing κ .
The quark mass was not kept constant !

Chiral crossover temperature $T_\chi \approx 230$ MeV was determined with a corresponding pion mass value of $O(1$ GeV).

T -dependence of the topological susceptibility in the interval $[0.85 T_\chi, 1.26 T_\chi]$ was studied by overimproved cooling for ensembles of 500 or 200 configurations. Volume effects are strong !

JINR-ITEP-IHEP-HU group has confronted the T -dependence of QCD with $N_f = 2$ with pure $SU(3)$ Yang-Mills theory (gluonic Wilson action).

Topology across the finite temperature transition studied by overimproved cooling in gluodynamics and QCD

V. G. Bornyakov, E.-M. Ilgenfritz, B. V. Martemyanov, V. K. Mitrjushkin, M. Müller-Preussker, **PRD 87 (2013) 114508** e-Print: arXiv:1304.0935

Cross-over in terms of topological susceptibility

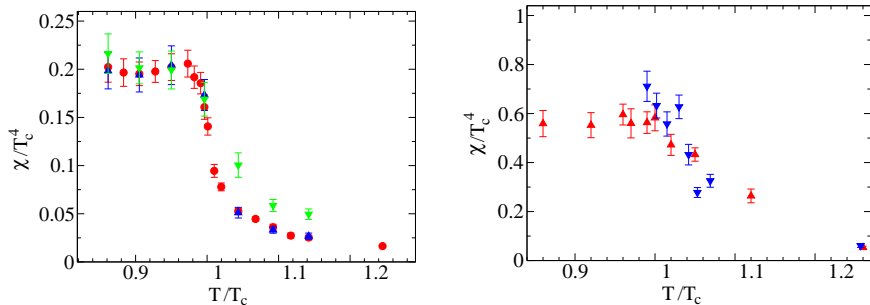


Figure: Left: topological susceptibility for gluodynamics on the lattices $16^3 * 4$ (red circles), $24^3 * 4$ (blue up triangles) and $24^3 * 6$ (green down triangles). Right: susceptibility for full QCD on the lattices $16^3 * 8$ (red up triangles) and $24^3 * 8$ (blue down triangles).

Two selected temperatures

For the two temperatures $T = T_\chi$ and $T = 1.06 T_\chi$, we recall the **topological susceptibilities** we have found (in PRD 87 (2013) 114508) by overimproved cooling:

ensemble I:

500 configurations, overimproved cooling, $\chi_{\text{top}} = (0.6 \pm 0.05) T_\chi^4$;

ensemble II:

200 configurations, overimproved cooling, $\chi_{\text{top}} = (0.3 \pm 0.03) T_\chi^4$.

Overlap study of topological susceptibility and topological structure

From the average square of the number of zero modes (equal to $\langle Q^2 \rangle$) we found:

at $T = T_\chi$ (ensemble I of 50 configurations $16^3 \times 8$)

$$\chi_{\text{top}} = (0.71 \pm 0.17) T_\chi^4;$$

at $T = 1.06 T_\chi$ (ensemble II of 50 configurations $24^3 \times 8$)

$$\chi_{\text{top}} = (0.24 \pm 0.05) T_\chi^4.$$

Difference within 4 or 6 % for the fourth root of the susceptibility specifies the systematical error induced by the cooling method.

New ideas put into the investigation of structure:

- no fixed number of non-zero eigenmodes
- replaced by variable eigenvalue cutoff
- using gradient flow to adapt the gluon field to the fermionic scale

Cutoffs

Ensemble I of 50 configurations $16^3 \times 8$ at $T = T_\chi$: $\lambda_{\text{sm}} = 331$ MeV.
(minimal spread of $|\lambda|$ among 20 non-zero eigenvalues per configuration)

Ensemble II of 50 configurations $24^3 \times 8$ $T = 1.06 T_\chi$: $\lambda_{\text{sm}} = 254$ MeV
(minimal spread of $|\lambda|$ among 30 non-zero eigenvalues per configuration)

In the case of ensemble I we also considered the smaller cutoff $\lambda_{\text{sm}} = 254$ MeV known from ensemble II.

This will allow us to discuss the effect of changing the cutoff for ensemble I (representing lower temperature) and to compare between the two temperatures (applying the smaller cutoff both to ensemble I and ensemble II).

The actual number of non-zero modes falling into these intervals and included into the definition of the topological density fluctuates from configuration to configuration.

The **fermionic topological density** depends on the **cutoff** λ_{sm} .

The **gluonic topological density needs smoothing**, for example by **gradient flow**, until it is adapted to the scale λ_{sm} .

Overimproved action (M. Garcia Perez, A. Gonzalez-Arroyo, J. Snippe, P. van Baal)

$$S(\epsilon) = \sum_{x,\mu\nu} \frac{4-\epsilon}{3} \text{Re Tr} (1 - U_{x,\mu\nu}) + \sum_{x,\mu\nu} \frac{1-\epsilon}{48} \text{Re Tr} (1 - U_{x,\mu\nu}^{2 \times 2})$$

One-instanton action (stabilizing instantons against shrinking)

$$S(\epsilon) = 8\pi^2 \left[1 - \frac{\epsilon}{5} \left(\frac{a}{\rho} \right)^2 + \mathcal{O} \left(\left[\frac{a}{\rho} \right]^4 \right) \right]$$

Overimproved cooling or gradient flow performed with $\epsilon = -1$.

Overimproved gradient flow

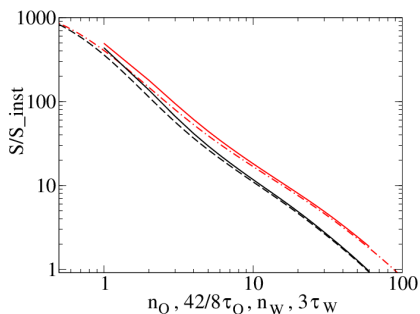


Figure: The evolution of action (in instanton units) with Wilson cooling step n_W (black line) and with Wilson flow time $3\tau_W$ (black dashed line) shown on the abscissa, and the evolution (in the same units) with overimproved cooling step n_O (red line) and with overimproved flow time $(42/8)\tau_O$ shown on the abscissa (red dash-dotted line).

Comparison of gluonic and fermionic topological density

$$q_{gluonic}(x) \rightarrow \tilde{q}_{gluonic} = q_{gluonic}(x) - \bar{q}_{gluonic}$$

$$q_{fermionic}(x) \rightarrow \tilde{q}_{fermionic} = q_{fermionic}(x) - \bar{q}_{fermionic}$$

The **similarity** between both topological densities is **expressed by** :

$$\cos(\theta) = \frac{\sum_x \tilde{q}_{gluonic}(x) \tilde{q}_{fermionic}(x)}{\sqrt{\sum_x \tilde{q}_{gluonic}(x)^2 \sum_x \tilde{q}_{fermionic}(x)^2}}$$

The **gradient flow** leads ...

- to a maximum of similarity between the two densities (stopping criterion = maximum of $\cos(\theta)$)
- to a maximum of localization of the gluonic topological density (in most cases reached before stopping)

Matching the scale-dependent fermionic topological density by the gluonic one : result of gradient flow

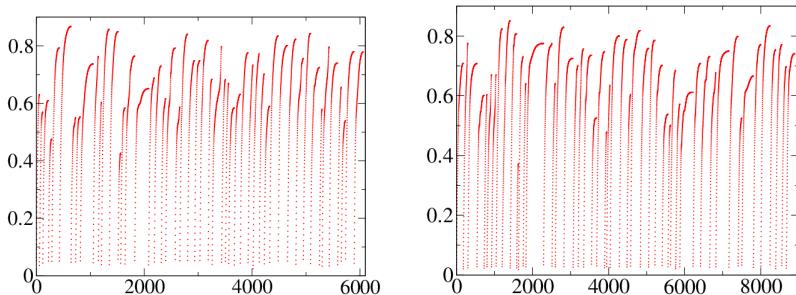


Figure: The evolution of the cosine $\cos(\theta)$, the cosine of an “angle” between gluonic and fermionic topological charge density, shown as function of flow time $(\tau_O/\Delta\tau)$, consecutively for all 50 configurations of ensemble I (left panel) and of ensemble II (right panel).

A measure of localization of the gluonic topological density

Inverse participation ratio continuously measured during gradient flow :

$$IPR = V_4 \frac{\sum_x |q(x)|^2}{(\sum_x |q(x)|)^2}$$

The localization of the gluonic topological density as result of gradient flow

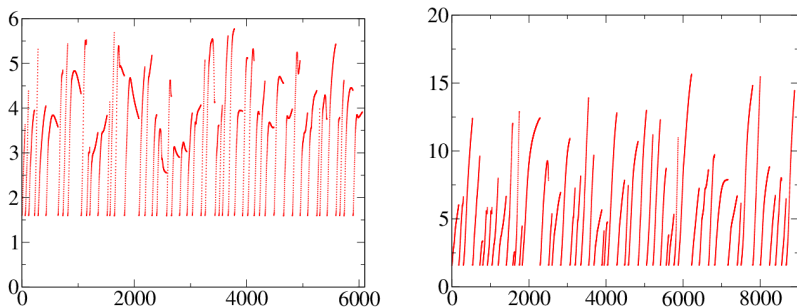


Figure: The inverse participation ratio IPR evolving in the course of over-improved gradient flow ($\tau_O/\Delta\tau$) until the best matching between gluonic topological charge density and fermionic topological charge density (averaged over boundary conditions) is achieved. Shown for all 50 configurations of the ensemble I (left panel) and ensemble II (right panel).

Flow time necessary to match the gluonic topological density to the (averaged) fermionic one

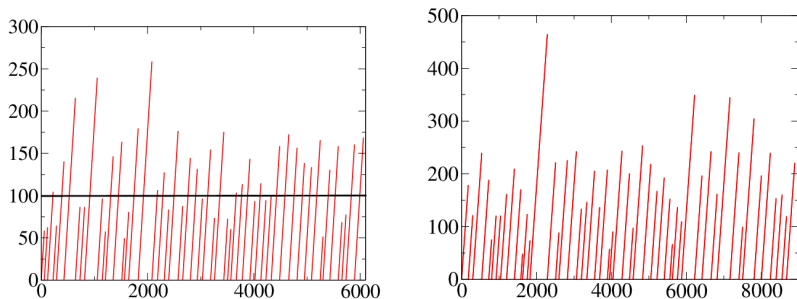


Figure: The number of steps of over-improved gradient flow ($\tau_O/\Delta\tau$) (with step size $\Delta\tau = 0.02$) until the cosine reaches the maximum (i. e. best matching is achieved). Shown for all 50 configurations of the ensemble I (left panel) and ensemble II (right panel).

A remarkable coincidence

The average number ≈ 100 of steps of length $\Delta\tau_O = 0.02$ in confinement corresponds to a diffusion length $a\sqrt{8\tau_O}$, which corresponds to the size of a dyon $1/(2\pi\nu_d T)$ in the confinement phase, when all $\nu_d = 1/3$.

The average value of $t_O^2 \frac{1}{2} \text{Tr}(F_{\mu\nu} F_{\mu\nu})$ is equal to 0.37 (with $t_O = a^2\tau_O$) which is close to the generally adopted stopping criterion.

Localization properties

type of BC	ensemble I $\lambda_{\text{sm}} = 331 \text{ MeV}$	ensemble I $\lambda_{\text{sm}} = 254 \text{ MeV}$	ensemble II $\lambda_{\text{sm}} = 254 \text{ MeV}$
1-st type b.c.	2.279(30)	2.373(36)	3.312(76)
2-nd type b.c.	2.282(29)	2.428(36)	3.259(84)
3-rd type b.c.	2.354(35)	2.493(45)	8.436(964)

Table: Inverse Participation Ratio (IPR) of the fermionic topological charge density at the selected fermionic cutoffs λ_{sm} , for three types of boundary conditions.

Cluster properties at T_χ Clusters obtained with lowest overlap modes for $16^3 \times 8$ configurations

Type	V_{cl}	V_{clmon}	N_{cl}	N_{clmon}	N_{moncl}	N_{loopcl}
1-st type	6.7(8)%	6.1(8)%	12.9(3)	3.5(2)	32(3)	5.4(4)
2-nd type	6.0(7)%	5.2(7)%	13.1(3)	3.7(2)	30(2)	5.4(4)
3-d type	6.1(8)%	5.5(8)%	12.0(4)	3.6(2)	31(2)	5.1(4)
all (331 MeV)	11(1)%	10(1)%	38(1)	10.8(6)	45(3)	6.4(4)
all (254 MeV)	12(1)%	11(1)%	32(1)	9.6(6)	42(3)	5.8(4)

Cluster properties above T_χ Clusters obtained with lowest overlap modes for $24^3 \times 8$ configurations

Type	V_{cl}	V_{clmon}	N_{cl}	N_{clmon}	N_{moncl}	N_{loopcl}
1-st type	5.1(3)%	4.4(4)%	24(1)	5.8(3)	59(3)	9.9(6)
2-nd type	6.2(6)%	5.5(6)%	24(1)	5.5(3)	64(4)	10.6(7)
3-d type	1.8(2)%	1.5(2)%	11(1)	5.7(4)	40(3)	6.7(6)
all (254 MeV)	8.0(6)%	7.0(6)%	59(2)	17.0(8)	76(5)	12.1(7)

Weyl plots

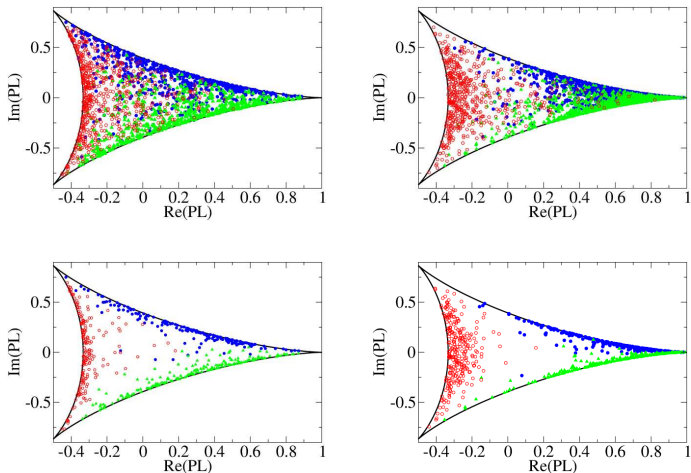


Figure: Scatter plots of Polyakov loop PL (after over-improved gradient flow) in the centers of all clusters (upper row) and of clusters selected to contain monopoles (lower row). Left: all clusters in all 50 configurations of ensemble I ($T = 1.0T_\chi$). Right: the same for ensemble II ($T = 1.06T_\chi$). Clusters separated according to boundary condition for the overlap near-zero modes. First type clusters green triangles, second type clusters blue filled circles, third type clusters red open circles.

Summary

- Topological lumps different from instantons are probably important for generating confinement.
- The three kinds may differ from each other. Localization and relative suppression are particular properties related to antiperiodic BC above T_c .
- The three kinds can be made visible in separation by different BC for the overlap Dirac operator of valence quarks.
- These features are probably useful for the Anderson-like scenario of the QCD chiral transition :
discussed in papers of M. Giordano, T. G. Kovacs, F. Pittler et al.
arXiv:1312.1179, arXiv:1312.1949, arXiv:1410.8308,
arXiv:1410.8392, arXiv:1507.02162, arXiv:1603.09548

Outline

- 1 Introduction: Cooling and vacuum structure
- 2 Conditions for “freeze-out” of numerical solutions for SU(2)
- 3 Analytical caloron and dyon solutions (for arbitrary SU(N))
- 4 Conditions for “freeze-out” of SU(3) calorons and dyons
- 5 Why calorons ? Can calorons generate confinement ?
- 6 Overlap analysis of dyon structure in gluodynamics below/above T_{dec}
- 7 Overlap analysis of dyon structure in dynamical QCD at/above T_{χ}
- 8 Outlook and Plans**

Interesting topological effects in QCD with dynamical fermions

- Effect of external magnetic fields on the topological structure in different phases (mediated to gluons via dynamical fermions) ? This was the original motivation in the Berlin group for developing the SU(2) HMC code (now under further development in ITEP).
- Effect of different chemical potentials (baryonic μ_B and chiral μ_5) on the topological structure ? For SU(2) planned in collaboration with V. Braguta, A. Kotov and A. Nikolaev (ITEP, FEFU).
- Roberge-Weiss transition : imaginary chemical potential μ_B in SU(3) QCD and first order phase transitions between different types of dyons (work is in progress in collaboration with B. Martemyanov, V. Bornyakov, A. Nikolaev (ITEP, FEFU))

In progress: Roberge-Weiss transition and topology

SU(3) simulations at imaginary chemical potential

lattice size : $L_S = 16$ and $L_T = 4$

lattice setting : WHOT-QCD :

- SU(3) Iwasaki gauge action
- $N_f = 2$ improved Wilson fermions, C_{SW} perturbatively determined
- pion mass chosen : $m_\pi/m_\rho = 0.8$
- $T/T_\chi = 1.35$
- imaginary chemical potential $\mu_B = i\mu_I$

In progress: Roberge-Weiss transition and topology

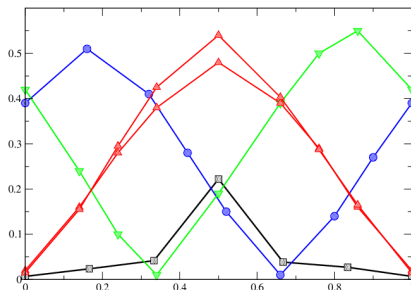


Figure: Gap of the overlap spectrum vs. angle ϕ entering the BC for overlap valence quarks.

Red curve (higher): $\mu_I/T = 0.0$

Red curve (lower): $\mu_I/T = 1.0 \lesssim 2\pi/6$

Blue curve: $\mu_I/T = 1.1 \gtrsim 2\pi/6$

Green curve: $\mu_I/T = 3.2 \gtrsim 2\pi/3$

Black curve: artificial configuration two dyon-antidyon pairs (of type 1 and type 2)